Report

A20 controls RANK-dependent osteoclast formation and bone physiology

Arne Martens[1,2], Pieter Hertens[1,2] iD, Dario Priem[1,2], Vagelis Rinotas[3] iD, Theodore Meletakos[3], Meropi Gennadi[3], Lisette Van Hove[1,2], Els Louagie[1,4], Julie Coudenys[1,4], Amélie De Muynck[5], Djoere Gaublomme[1,4], Mozes Sze[1,2], Jolanda van Hengel[6] iD, Leen Catrysse[1,2], Esther Hoste[1,2] iD, Jeffrey D Zajac[7], Rachel A Davey[7], Luc Van Hoorebeke[5], Tino Hochepied[1,2], Mathieu J M Bertrand[1,2] iD, Marietta Armaka[3] iD, Dirk Elewaut[1,4] iD & Geert van Loo[1,2,*] iD

Abstract

The anti-inflammatory protein A20 serves as a critical brake on NF–κB signaling and NF–κB-dependent inflammation. In humans, polymorphisms in or near the *TNFAIP3/A20* gene have been associated with several inflammatory disorders, including rheumatoid arthritis (RA), and experimental studies in mice have demonstrated that myeloid-specific A20 deficiency causes the development of a severe polyarthritis resembling human RA. Myeloid A20 deficiency also promotes osteoclastogenesis in mice, suggesting a role for A20 in the regulation of osteoclast differentiation and bone formation. We show here that osteoclast-specific A20 knockout mice develop severe osteoporosis, but not inflammatory arthritis. *In vitro*, osteoclast precursor cells from A20 deficient mice are hyperresponsive to RANKL-induced osteoclastogenesis. Mechanistically, we show that A20 is recruited to the RANK receptor complex within minutes of ligand binding, where it restrains NF–κB activation independently of its deubiquitinating activity but through its zinc finger (ZnF) 4 and 7 ubiquitin-binding functions. Together, these data demonstrate that A20 acts as a regulator of RANK-induced NF–κB signaling to control osteoclast differentiation, assuring proper bone development and turnover.

Introduction

Bone is continuously being remodeled in a process of bone matrix synthesis by osteoblasts and bone resorption by osteoclasts (Zaidi, 2007; Chang *et al*, 2009). This is a highly regulated process requiring "coupling" of bone resorption and reformation, and perturbations in this balance lead to a loss in bone mineral density, a disease called osteoporosis, or in too dense bones, known as osteopetrosis (Wada *et al*, 2006). Osteoclasts are large, multinucleated cells formed by the cytoplasmatic fusion of cells that differentiate from the macrophage/monocyte lineage (Itzstein *et al*, 2011). Activated mature osteoclasts adhere to the bone surface and form tightly sealed compartments with the bone surface, called resorption pits, in which osteoclasts release lytic enzymes such as tartrate-resistant acid phosphatase (TRAP) and pro-cathepsin K, next to hydrogen ions to acidify the environment (Boyle *et al*, 2003).

Osteoclastogenesis critically relies on two factors, *viz.* macrophage colony-stimulating factor (M-CSF) and receptor activator of Nuclear Factor–κB (RANK) ligand (RANKL), which are sufficient to induce osteoclast differentiation *in vitro* (Quinn *et al*, 1998). Binding of RANKL to its receptor RANK, a member of the tumor necrosis factor (TNF) receptor superfamily expressed on the surface of osteoclast precursors, recruits the adaptor protein TRAF6, which induces the activation of several downstream signaling pathways leading to the activation of the transcription factors Nuclear Factor–κB (NF–κB) and activator protein-1 (AP-1). RANK signaling also induces the activation of Nuclear Factor-Activated T cells c1 (NFATc1), the so called "master regulator of osteoclast differentiation," responsible for the expression of critical osteoclast genes coding for TRAP, cathepsin K and the calcitonin receptor (CalcR; Takayanagi *et al*, 2002; Asagiri & Takayanagi, 2007; Tsukasaki & Takayanagi, 2019).

1 Center for Inflammation Research VIB, Ghent, Belgium
2 Department of Biomedical Molecular Biology, Ghent University, Ghent, Belgium
3 Biomedical Sciences Research Center 'Alexander Fleming', Vari, Greece
4 Department of Rheumatology, Ghent University Hospital, Ghent, Belgium
5 Department of Physics and Astronomy, Ghent University, Ghent, Belgium
6 Department of Human Structure and Repair, Ghent University, Ghent, Belgium
7 Department of Medicine, Austin Health, University of Melbourne, Heidelberg, Victoria, Australia
*Corresponding author. Tel: +003293313761; Fax: +003292217673; E-mail: geert.vanloo@irc.vib-ugent.be; geert.vanloo@ugent.be

The NF–κB family of transcription factors plays critical roles in a wide variety of cellular processes, of which inflammation is the best described. Several mechanisms are known to control NF–κB activation assuring a tight control of the inflammatory response. The anti-inflammatory protein A20 (also known as Tumor Necrosis Factor Alpha-Induced Protein 3, TNFAIP3) is one of the key molecules involved in the regulation of NF–κB signaling and inflammatory gene expression (Martens & van Loo, 2020). Genetic deletion of *A20/Tnfaip3* in mice leads to a lethal multi-organ inflammation, confirming the importance of A20 in the repression of inflammatory responses (Lee *et al*, 2000). Myeloid-specific A20 deficiency in mice results in the spontaneous development of a severe destructive polyarthritis with many features of rheumatoid arthritis (RA; Matmati *et al*, 2011), and single nucleotide polymorphisms in the human *TNFAIP3* locus are associated with increased susceptibility to RA (Plenge *et al*, 2007; Thomson *et al*, 2007). Finally, *TNFAIP3* variants were recently shown to be shared between RA and varying osteoporotic phenotypes (Kasher *et al*, 2021).

In addition to its role in inflammation, A20 regulates developmental processes controlled by NF–κB signaling. For instance, we previously identified A20 as a negative regulator of NF–κB signaling downstream of the Ectodysplasin A receptor (EDAR), a pathway important for the development of epidermal appendages (Lippens *et al*, 2011). Since NF–κB is important for osteoclast differentiation, and NF–κB inhibition was shown to block osteoclastogenesis (Novack, 2011), A20 may, therefore, also play a direct role in the regulation of RANK-dependent NF–κB signaling and osteoclast formation. Such a role was reported for Cylindromatosis (CYLD), a deubiquitinating enzyme that negatively regulates RANK signaling and osteoclastogenesis (Jin *et al*, 2008). Accordingly, CYLD deficient mice develop severe osteoporosis due to aberrant osteoclast formation and activation. In line with the potential role of A20 in regulating RANK-induced NF–κB signaling, A20 deficiency was shown to promote osteoclastogenesis, since more TRAP-positive multinucleated osteoclasts could be detected at the outer bone surface in histological sections of ankle joints of myeloid-A20–deficient mice (Matmati *et al*, 2011). However, the enhanced osteoclastogenesis observed in myeloid A20 knockout mice may alternatively be the result of the more global inflammatory state of these mice, since inflammatory cytokines including TNF, IL-1β, IL-6, and IL-23 were previously shown to promote osteoclastogenesis (Dai *et al*, 2000; Lam *et al*, 2000; Ju *et al*, 2008; Levescot *et al*, 2021).

To characterize the exact role of A20 in osteoclastogenesis, we generated transgenic mice with osteoclast-specific A20 deficiency. We show that these mice spontaneously develop severe osteoporosis without the inflammatory component seen in myeloid-A20-deficient mice, thereby uncoupling the inflammatory and bone-specific phenotypes. We identified A20 as a new component of the RANK signaling complex that represses RANK-induced NF–κB signaling, osteoclast differentiation, and bone formation.

Results and Discussion

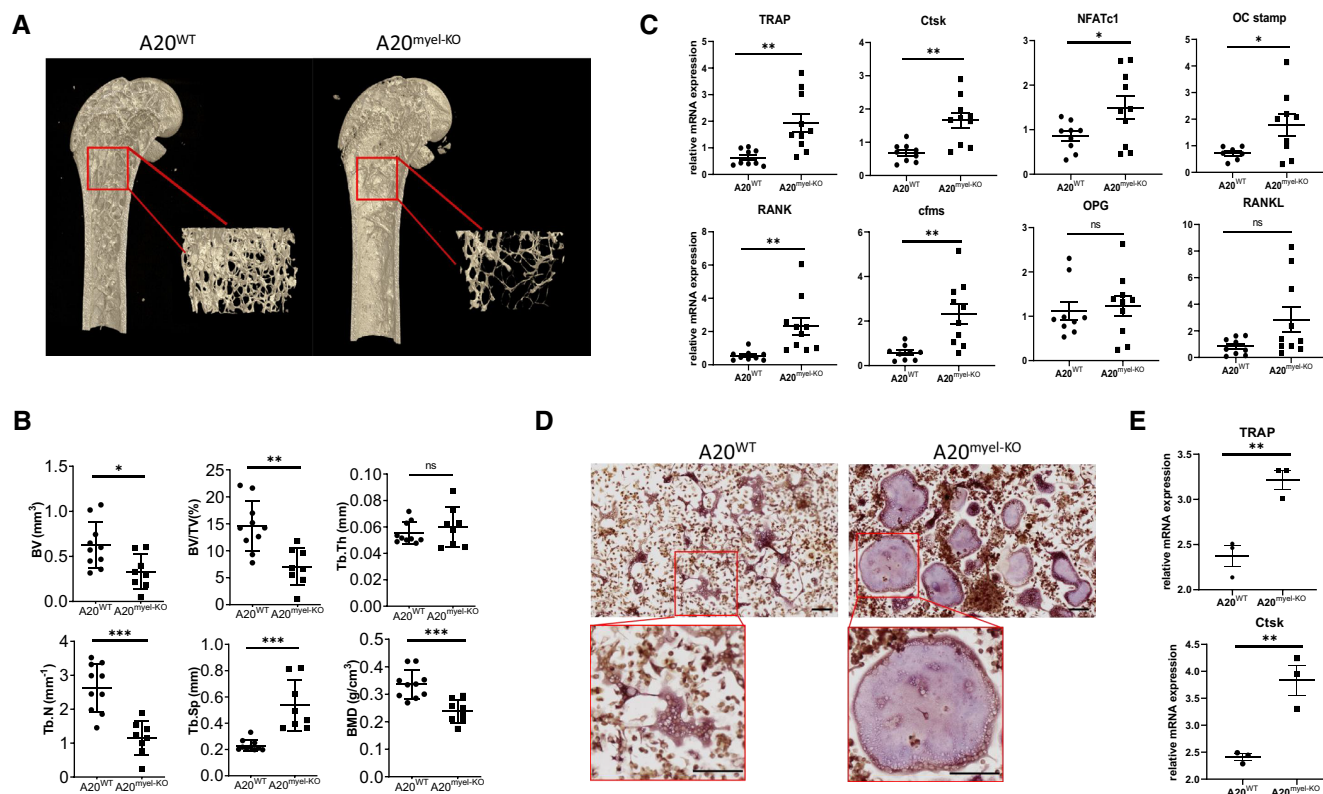## Myeloid-specific A20 deficiency promotes osteoclastogenesis

Myeloid-specific A20 deficient (A20[myel-KO]) mice spontaneously develop a severe destructive polyarthritis with many features of

human RA (Matmati *et al*, 2011). This inflammatory phenotype was shown to be caused by necroptosis of A20-deficient macrophages triggering inflammasome activation and release of IL-1α and IL-1β. Synovial fibroblasts respond to these cytokines secreted by the A20-deficient myeloid cells in the joints, further driving the inflammatory response leading to the development of arthritis (Vande Walle *et al*, 2014; Polykratis *et al*, 2019). Myeloid A20-deficient mice also show an expansion of peripheral CD115^{+}CD117^{+} osteoclast precursors, and blood leukocytes isolated from these mice produce more and larger osteoclasts *in vitro* upon incubation with RANKL and M-CSF than cells derived from wild-type mice (Matmati *et al*, 2011). These findings suggest that A20 deficiency promotes osteoclastogenesis. Indeed, *ex vivo* micro-computed tomography (microCT) analysis of femurs of A20[myel-KO] mice clearly shows severe loss of trabecular bone mass in these mice compared to control mice (Fig 1A and B). Similar differences could be observed for cortical bone parameters (Fig EV1A and B). Furthermore, gene expression analysis on ankle joints isolated from A20[myel-KO] and control littermate mice demonstrates a significant increase in expression of osteoclast-specific markers in A20[myel-KO] tissue compared to that of control wild-type mice, while no differences were observed for the expression of RANKL or its antagonist OPG (Fig 1C). *In vitro*, incubation of A20[myel-KO] bone marrow cells with RANKL and M-CSF generates significantly larger osteoclasts which contain substantially more nuclei than cells derived from wild-type progenitor cells (Fig 1D), as shown before using blood leukocytes (Matmati *et al*, 2011). In agreement, qPCR analysis confirms an increased expression of the osteoclast-specific markers TRAP and Ctsk in A20-deficient cells after 5 days of differentiation (Fig 1E). Together, these data demonstrate that increased osteoclast differentiation in the absence of A20 might contribute to the severe bone osteoporosis in myeloid A20-deficient mice.

Osteoclast-specific A20 deficient mice develop severe osteoporosis

Myeloid A20–deficient mice show high serum levels of TNF and IL-6 (Matmati *et al*, 2011; Fig 2A), inflammatory and RA-associated cytokines known to promote osteoclastogenesis (Dai *et al*, 2000; Lam *et al*, 2000). To address if A20 plays a direct regulatory role in RANK-induced signaling and osteoclastogenesis, we generated transgenic mice with osteoclast-specific A20 deficiency by crossing the floxed *A20* line (Vereecke *et al*, 2010) with mice expressing Cre recombinase under the control of the *Cathepsin K* promoter, which is selectively active in differentiated osteoclasts (Chiu *et al*, 2004). Osteoclast-specific A20-deficient (A20[OC-KO]) mice develop normally and do not display swelling and redness of the front and hind paws nor other signs of arthritis development as seen in A20[myel-KO] mice. Also, and in contrast to A20[myel-KO] mice, A20[OC-KO] mice do not have elevated levels of inflammatory cytokines in their serum (Fig 2A). To investigate the consequence of osteoclast-specific A20 deletion for bone physiology, we next analyzed the structure, bone mass and bone density of femurs of A20[OC-KO] and control littermate mice by microCT analysis. Twenty to thirty week old A20[OC-KO] mice display severe loss of trabecular bone, compared to wild-type mice (Figs 2B and EV2A). In agreement, the volume and density of trabecular bone is significantly reduced in A20[OC-KO] mice (Figs 2C and EV2B). However, no

Figure 1. Myeloid-specific A20 deficiency promotes osteoclastogenesis.

A Representative micro-CT pictures of hind legs of 20–30 week old control (A20[WT]) and A20[myel-KO] littermates. Note the severe osteoporosis in A20[myel-KO] mice.

B Trabecular parameters, calculated on micro-CT scans of hind legs of 20–30 week old control (A20[WT]) and A20[myel-KO] littermates. Each dot represents an individual mouse (A20[WT], $n = 10$; A20[myel-KO], $n = 8$). Data are expressed as mean $\pm$ SEM. *, **, *** represent $P < 0.05$, $P < 0.01$, $P < 0.001$, respectively (parametric unpaired t-test).

C qRT–PCR mRNA expression analysis of osteoclast-specific genes on RNA isolated from ankles of mice with the indicated genotypes (A20[WT], $n = 9$; A20[myel-KO], $n = 10$). Data are expressed as mean $\pm$ SEM. * and ** represent $P < 0.05$, $P < 0.01$, respectively (parametric unpaired t-test).

D TRAP staining on osteoclast cultures derived from bone marrow cells isolated from tibia of A20[WT] and A20[myel-KO] mice and incubated for 7 days with M-CSF (25 ng/ml) and RANKL (100 ng/ml). Scale bar, 100 μm.

E qRT–PCR mRNA expression analysis on RNA isolated from bone marrow cultures from A20[WT] and A20[myel-KO] mice, incubated with M-CSF (25 ng/ml) and RANKL (100 ng/ml) for 5 days to induce osteoclastogenesis (A20[WT], $n = 3$; A20[myel-KO], $n = 3$). Data are expressed as mean $\pm$ SEM. ** represents $P < 0.01$ (the Kruskal–Wallis one-way ANOVA test between indicated genotypes).

Source data are available online for this figure.

significant differences between A20[OC-KO] and control mice could be observed for cortical bone parameters (Fig EV2C and D). Next, we tested the strength of the femoral diaphysis by measuring the ultimate load until failure (N) via a three-point bending test, representing the highest force the bone can withstand. A20[OC-KO] bones require significantly less force before they break compared to bones from wild-type mice, as could be expected based on the severe bone loss observed by microCT analysis (Figs 2D and EV2E). Finally, histological analysis of the tibia of 20 week old mice shows significantly more TRAP-positive osteoclasts in A20[OC-KO] mice compared to control littermates (Fig 2E and F). Although old mice (50 weeks of age) have reduced numbers of osteoclasts present in their tibia, A20[OC-KO] mice still have significantly more osteoclasts than wild-type controls of the same age (Fig EV2F and G). Contrary to A20[myel-KO] mice (Matmati *et al*, 2011), A20[OC-KO] mice do not show an expansion of peripheral CD115+CD117+

osteoclast precursors (Fig EV3A and B). Together, these data demonstrate that A20 directly regulates osteoclast formation *in vivo*, independent of its anti-inflammatory functions.

A20 regulates RANK-induced NF-κB activation

We next assessed the consequence of osteoclast-specific A20 deletion for RANK-induced signaling *in vitro*. Although no significant difference is observed in the number of TRAP-positive osteoclasts or in osteoclast activity in A20[OC-KO] primary cultures compared to wild-type control cultures after incubation with M-CSF and RANKL, A20[OC-KO] cells show a trend towards more osteoclasts (Figs 3A and EV4A–C). Also, increased expression of the osteoclast-specific markers TRAP and Ctsk can be detected in A20[OC-KO] cultures (Fig 3B). However, no significant increase in expression of inflammatory cytokines is observed (Fig EV4D and E).

In most cell types, A20 expression levels are low at a steady state, but are rapidly upregulated in inflammatory conditions as a result of NF–κB activation (Krikos *et al*, 1992). In the process of osteoclastogenesis, A20 expression is also upregulated upon incubation of cells with RANKL, suggesting that *A20* is an NF–κB response gene acting as a negative feedback regulator of RANK-induced NF–κB signaling (Fig 3C). Indeed, using an NF–κB-dependent luciferase reporter assay in HEK293T cells, we demonstrate that A20 blocks RANK-induced activation of NF–κB (Fig 3D). In agreement, A20 deficient bone marrow-derived macrophages (BMDMs) show
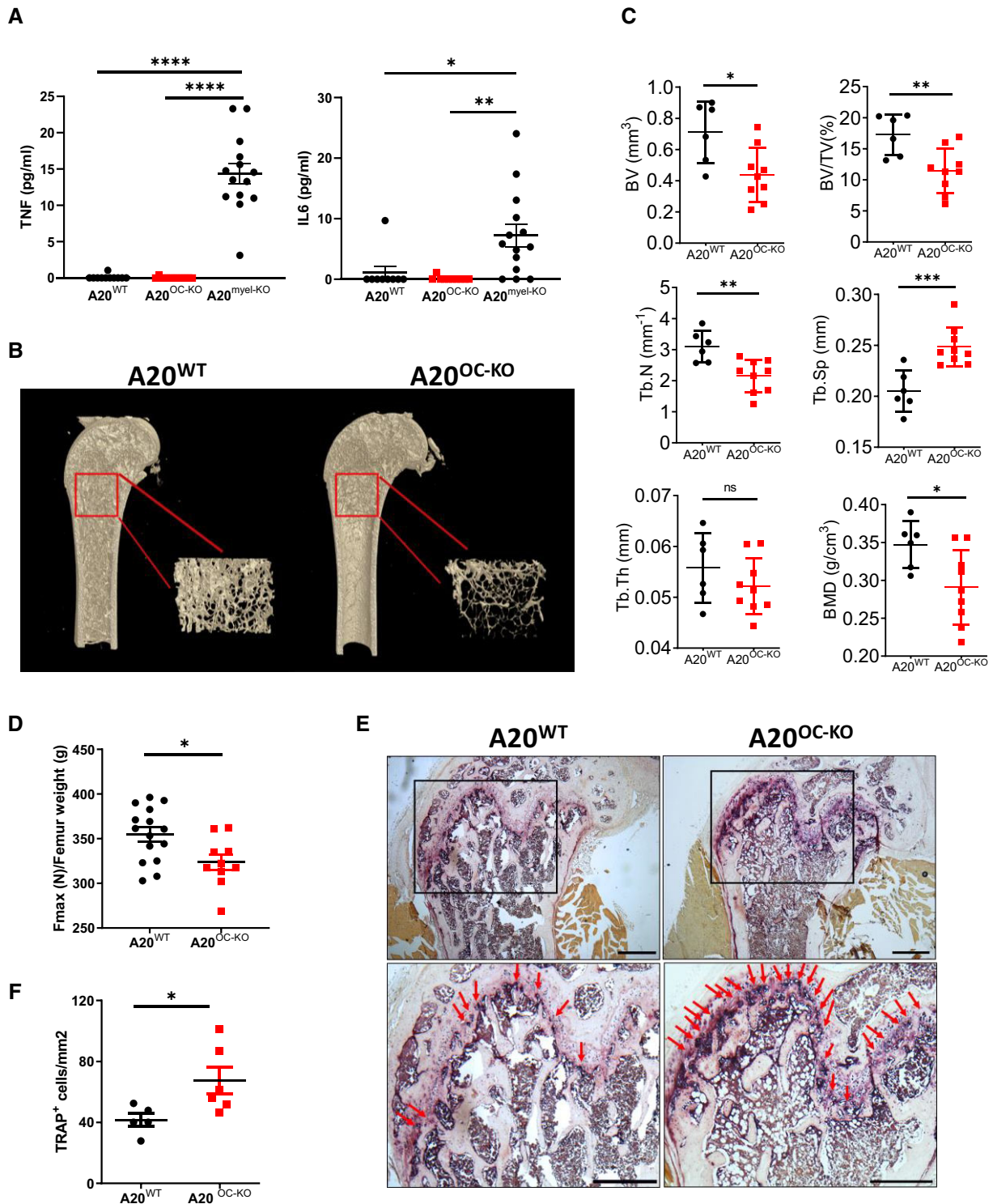

Figure 2.

Figure 2. Osteoclast-specific deletion of A20 in mice induces severe osteoporosis and enhanced osteoclastogenesis.

A Levels of TNF and IL-6 in serum of A20[WT], A20[OC-KO], and A20[myel-KO] mice. Each dot represents an individual mouse (A20[WT], *n* = 11; A20[OC-KO], *n* = 11 and A20[myel-KO], *n* = 14). Data are expressed as mean ± SEM. * represents *P* < 0.05, ** *P* < 0.01, **** *P* < 0.0001, n.s. nonsignificant (parametric one-way ANOVA between indicated genotypes).

B Representative micro-CT pictures of hind legs of 20–30 week old control (A20[WT]) and A20[OC-KO] littermates. Note the severe osteoporosis in A20[OC-KO] mice.

C Trabecular parameters, calculated on micro-CT scans of hind legs of 20–30 week old control (A20[WT]) and A20[OC-KO] littermates. Each dot represents an individual mouse (A20[WT], *n* = 6; A20[OC-KO], *n* = 9). Data are expressed as mean ± SEM. *, **, *** represent *P* < 0.05, *P* < 0.01, *P* < 0.001, respectively; ns, nonsignificant (parametric unpaired *t*-test).

D Functional femur strength was determined by the three-point bending test and is expressed as the maximum force (Fmax, Newton) bones can resist before breaking, corrected for femur weight, with higher values mirroring stronger bones. Each dot represents an individual mouse (27 week old A20[WT], *n* = 9; A20[OC-KO], *n* = 6). Data are expressed as mean ± SEM. * represents *P* < 0.05 (the nonparametric Mann–Whitney test between indicated genotypes).

E Representative pictures of TRAP-stained sections from the tibia of 20 week old A20[WT] and A20[OC-KO] mice. Red arrows indicate osteoclasts. Scale bar, 500 μm.

F Quantification of the number of TRAP-positive cells on sections from the tibia of 20 week old A20[WT] and A20[OC-KO] mice. Each dot represents an individual mouse (A20[WT], *n* = 5; A20[OC-KO], *n* = 6). Data are expressed as mean ± SEM. * represents *P* < 0.05 (the nonparametric Mann–Whitney test between indicated genotypes).

Source data are available online for this figure.

increased NF–κB signaling in response to RANKL, as shown by stronger and prolonged IκBα phosphorylation and degradation and by stronger phosphorylation of p65, than wild-type cells (Fig 3E). Also increased phosphorylation of the MAP kinase p38 is observed in A20 deficient BMDMs in response to RANKL (Fig 3E). Similar to the recruitment of A20 to the TNF receptor (TNFR1) upon TNF sensing (Zhang *et al*, 2000; Draber *et al*, 2015; Priem *et al*, 2019; Martens *et al*, 2020), we found that A20 is also rapidly recruited to the RANK receptor upon stimulation of BMDMs with GST-tagged RANKL (Fig 3F). Moreover, TNF receptor–associated factor 6 (TRAF6), a crucial signaling adaptor that transduces the RANK-mediated signal, as well as HOIP and Sharpin, two proteins of the linear ubiquitin chain assembly complex (LUBAC) essential for linear ubiquitination, are more strongly recruited to the receptor in A20-deficient cells, indicative of increased RANK-induced signaling in A20-deficient conditions (Fig 3F). However, it needs to be noted that also more RANK is detected upon pulldown of the receptor complex in A20-deficient cells, suggesting that more receptors can signal (Fig 3F). In contrast, similar levels of the receptor are present in the lysates of A20 sufficient and deficient cells, as well as GST levels after pulldown of the receptor complex, suggesting that RANK levels are similar, but possibly less modified in the KO cells (Fig 3F).

Next to canonical NF–κB signaling, RANK activation is also known to induce activation of the noncanonical NF–κB pathway, which involves the processing of the NF–κB2 precursor protein p100 to generate p52 (Sun, 2017). Interestingly, A20 deficient BMDMs have higher levels of p100, a noncanonical NF–κB response protein (Lombardi *et al*, 1995; Fig 3G). Moreover, increased processing of p100 to p52 can be observed in A20 deficient BMDMs compared to wild-type cells upon treatment with RANKL, confirming increased activation of the noncanonical NF–κB pathway (Fig 3G). Together these results indicate that A20 is recruited to the RANK receptor upon ligand sensing, where it negatively regulates NF–κB signaling.

A20 inhibits RANK signaling via its ubiquitin binding function

We previously demonstrated that the anti-inflammatory and cyto-protective functions of A20 are largely dependent on its ubiquitin-binding properties (Martens *et al*, 2020). To unravel how A20 regulates RANK signaling, different A20 mutants were tested for their ability to suppress RANK-induced NF–κB activation in HEK293T cells. An A20 point mutant (C103A), which is critically mutated in its N-terminal deubiquitinating (DUB) activity (A20[DUB]), is as effective as wild-type A20 in inhibiting RANK-induced NF–κB activation,

Figure 3. A20 regulates RANK-induced NF–κB signaling.

A Bone marrow cells isolated from A20[WT] and A20[OC-KO] mice were cultured on glass coverslips for 7 days in α-MEM medium supplemented with M-CSF (25 ng/ml) alone or with M-CSF and RANKL (100 ng/ml). On day 7, osteoclasts were stained with TRAP. Scale bar, 50 μm.

B qRT–PCR mRNA expression analysis on RNA from bone marrow cultures isolated from A20[WT] and A20[OC-KO] mice and incubated for 6 days with M-CSF (25 ng/ml) and RANKL (100 ng/ml; time point 0 represents a 7 day culture with M-CSF alone). (A20[WT], *n* = 4–5; A20[OC-KO], *n* = 4–5). ** represent *P* < 0.05, *P* < 0.01, respectively (Two-way ANOVA test with Sidak's multiple comparisons between indicated genotypes for each time-point).

C qRT–PCR mRNA expression analysis on RNA from BMDM cultures isolated from control (A20[WT]) mice (*n* = 3) incubated for the indicated time-points with RANKL (100 ng/ml). Data are expressed as mean ± SEM.

D Measurement of NF–κB luciferase activity in lysates of HEK293T cells transiently transfected with an NF–κB reporter plasmid, an expression plasmid for β-galactosidase (βgal), an expression plasmid for RANK, and with either an empty vector or a vector expressing wild-type A20. Cell lysates were analyzed for luciferase, and βgal activity, and values are plotted as Luc/βgal to normalize for possible differences in transfection efficiency. Data are expressed as the mean of technical triplicates ± SD. **** represent *P* < 0.0001; ns, non-significant (Two-way ANOVA test with Sidak's multiple comparisons between indicated genotypes).

E Western blot analysis of whole cell lysates from BMDMs cultures isolated from A20[WT] and A20[myel-KO] mice and stimulated with RANKL (100 ng/ml) for the indicated time periods. Actin is shown as a loading control.

F Wild-type and A20 deficient BMDMs were stimulated with GST-RANKL (1 μg/ml) for the indicated time periods. The RANK signaling complex was immunoprecipitated using glutathione-sepharose beads and immunoblotted for RANK, A20, TRAF6, HOIP, and Sharpin.

G BMDMs from A20[WT] and A20[myel-KO] mice were stimulated with RANKL (100 ng/ml) for the indicated time periods and immunoblotted to visualize p100 processing to p52. Actin is shown as a loading control.
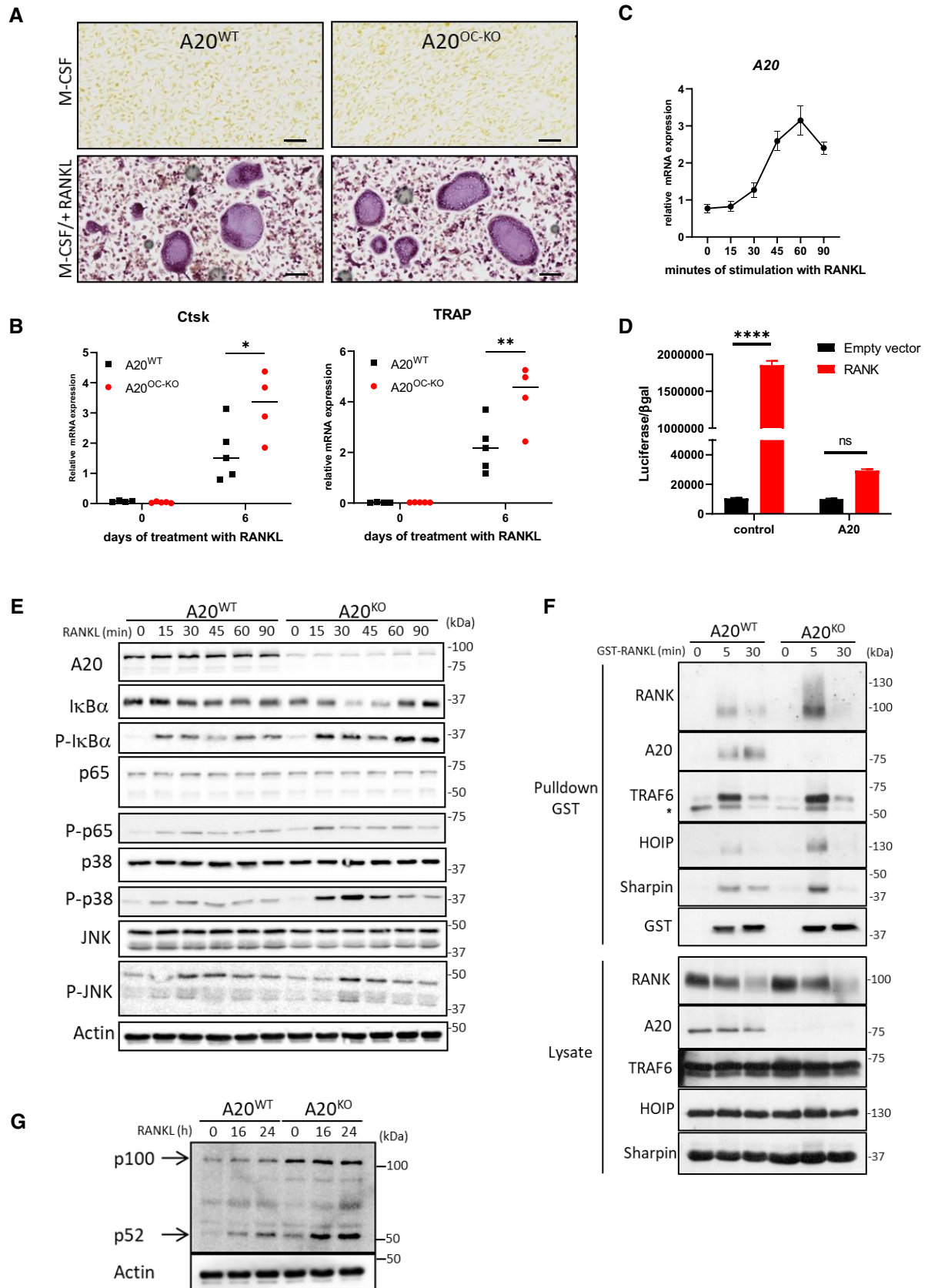
Source data are available online for this figure.
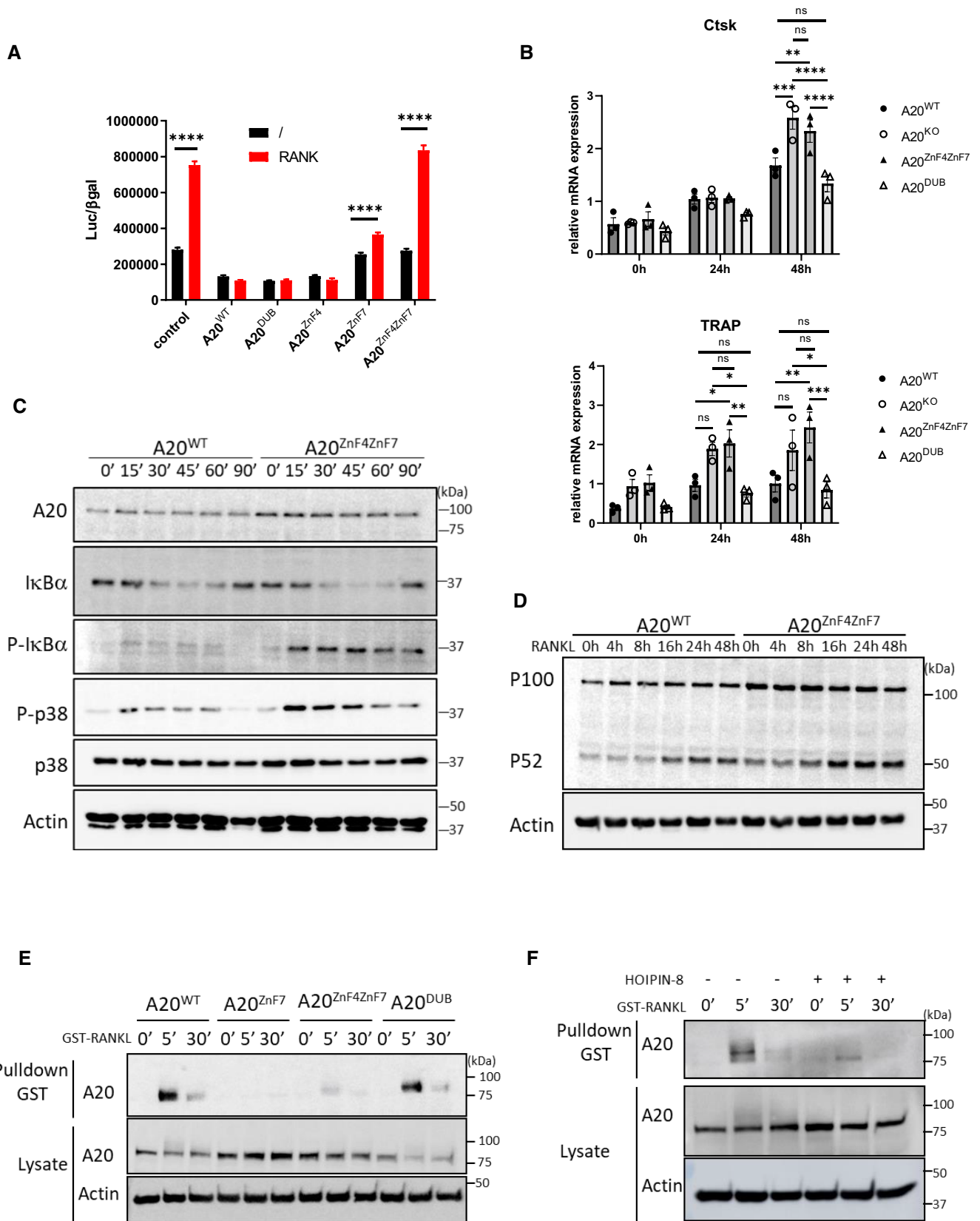
Figure 3.

A

B

C

D

E

F

Figure 4.

◀

indicating that the A20 DUB activity is not involved in the regulation of RANK signaling (Fig 4A). However, an A20 mutant mutated in its zinc finger 7 (ZnF7) domain (C775A/C779A; A20^{ZnF7}), which was previously shown to have high-binding affinity for linear ubiquitin (Tokunaga *et al*, 2012; Verhelst *et al*, 2012), shows slightly reduced NF–κB-inhibiting activity, while an A20 variant mutated in both its ZnF4 (C624A/C627A) and ZnF7 ubiquitin-binding domains (A20^{ZnF4ZnF7}) completely loses its ability to suppress RANK-induced NF–κB signaling (Fig 4A). In agreement, Ctsk and TRAP expression are only increased in BMDMs from A20^{ZnF4ZnF7} mice compared to wild-type or A20^{DUB} BMDMs, similar to what is seen in A20^{KO} cells (Fig 4B). These results indicate that A20 negatively regulates RANK-induced NF–κB activation via its ubiquitin-binding activities. This is further confirmed in A20^{ZnF4ZnF7} BMDMs, showing increased canonical and noncanonical NF–κB and p38 MAPK signaling upon stimulation with RANKL, as compared to BMDMs expressing wild-type A20 (Fig 4C and D).

A20 was previously shown to be recruited to the TNFR1 complex via binding of its ZnF7 domain to linear (M1) ubiquitin (Draber *et al*, 2015; Priem *et al*, 2019; Martens *et al*, 2020). A GST–RANKL pulldown assay on BMDMs from the different A20 mutant mice shows that ZnF7 mutation is sufficient to prevent A20 recruitment to the RANK signaling complex, while the DUB mutation does not affect A20 recruitment (Fig 4E). In agreement, LUBAC inhibition by treatment with HOIPIN-8, strongly prevents A20 recruitment (Fig 4F), confirming that M1 chains are needed to recruit A20 to the RANK receptor. Together these results demonstrate that A20 inhibits RANK-induced signaling via its ubiquitin binding properties.

In conclusion, our findings uncover a new role for A20 in the regulation of RANK-induced NF–κB signaling, osteoclast formation, and bone physiology. Hence, osteoclast-specific A20 deletion in mice causes the development of severe osteoporosis, characterized by increased numbers of TRAP$^+$ osteoclasts detected in bone tissue of A20 deficient mice. Absence of A20 in osteoclasts promotes RANK-induced NF–κB and p38 signaling, and enhances the expression of osteoclast-specific genes, demonstrating that A20 acts as a negative regulator of RANK signaling, similar to its function in the regulation of inflammatory signaling (Martens & van Loo, 2020; Fig EV5). The mechanism by which A20 regulates RANK signaling is, however, still unclear. Previous studies have shown that the deubiquitinating enzyme CYLD inhibits RANK-induced NF-κB activation by restricting TRAF6 ubiquitination (Jin *et al*, 2008). Although A20 has also been described to act as a deubiquitinating enzyme that controls NF-κB signaling by regulating the ubiquitination status of TRAF6 as well as other targets (Boone *et al*, 2004; Martens & van Loo, 2020), these findings have previously been questioned based on the phenotype of a transgenic mouse strain which bears an inactivating mutation in the A20 DUB domain (De *et al*, 2014). We also have no evidence that A20 regulates RANK activation via its DUB activity, since the expression of a catalytic C103R DUB mutant can still inhibit RANK-induced NF-κB signaling and osteoclast-specific gene expression, suggesting a nonenzymatic role for A20 in suppressing RANK signaling. Indeed, we could demonstrate that A20 variants mutated in their ability to bind ubiquitin via its ZnF4 and ZnF7 domains are no longer recruited to the RANK receptor complex, and hence cannot suppress RANK-induced NF–κB activation.

Materials and Methods

Mice

Conditional A20/*tnfaip3* knockout mice, in which exons IV and V of the *tnfaip3* gene are flanked by two LoxP sites, were generated as described before (Vereecke *et al*, 2010). A20 floxed mice were crossed with LysM-Cre (Clausen *et al*, 1999) or CathepsinK-Cre transgenic mice (Chiu *et al*, 2004) to generate a myeloid-specific (A20$^{myel-KO}$) or osteoclast-specific A20 knockout mouse (A20^{OC-KO}). Full-body A20^{ZnF7} knockin mice and myeloid-specific A20^{ZnF4ZnF7} knockin mice, containing the ZnF7 (C764A/C767A) or ZnF4 (C609A/C612A) and ZnF7 mutations, respectively, were previously described (Martens *et al*, 2020). A20^{DUB} knockin mice, that have a catalytic C103R mutation in the deubiquitinating OTU domain, were newly generated by CRISPR/Cas9 gene targeting. For this, Cas9 protein (VIB Protein Service Facility), together with a 123 bp single-stranded repair template (TGC < CGG (C103R): 5′ - TTGCTTTGGGC TGCTTAACCTTGCTCCTCACAGCTCCTTCTGTCCTCAGGTGATGGA AACCGGCTCATGCATGCAGCTTGTCAGTACATGTGGGGTGTTCAGG ATACTGACCTGGTCCTGAGG - 3′, iDT) and a short guide RNA (sgRNA, 5′- ACTGACAAGCTGCATGCATG −3′, iDT) targeting the

OTU domain of the murine *A20* gene, were electroporated into zygotes obtained from C57BL/6 mice. The embryos were transferred the same day to foster mothers through oviduct transfer.

All experiments were performed on mice of C57BL/6J genetic background. Mice were housed in individually ventilated cages at the VIB Center for Inflammation Research in a specific pathogen-free facility. All experiments on mice were performed according to institutional, national, and European animal regulations. Animal protocols were approved by the ethics committee of Ghent University (license reference number 2016-042 and 2017-042).

Isolation of bone marrow-derived macrophages

BMDMs were obtained from bone marrow cells flushed from mouse femurs and tibia with sterile RPMI medium, and cultured in RPMI 1640 supplemented with 40 ng/ml recombinant mouse M-CSF, 10% FCS, 1% penicillin/streptavidin, and glutamine. Fresh M-CSF was added on day 3, and medium was refreshed on day 5. On day 7, cells were seeded and stimulated with 100 ng/ml RANKL (Peprotech) for the indicated time points.

Isolation of bone marrow-derived osteoclasts

Osteoclasts were obtained from bone marrow cells flushed from mouse femurs and tibia with sterile RPMI medium, and cultured overnight in αMEM medium (Gibco) containing 20% FCS in a petridish. The next day, the cells were seeded on glass coverslips in αMEM medium containing 20% FCS, 25 ng/ml M-CSF and 100 ng/ml RANKL (Peprotech). The medium was refreshed on day 5, and on day 7, cells were stained or processed for further analysis. Alternatively, the cells were seeded on bovine bone slices (Immunodiagnostic Systems) in αMEM medium containing 20% FCS, 25 ng/ml M-CSF and 100 ng/ml RANKL (Peprotech). The medium was refreshed on days 6, 8, 10, and 12, and culture supernatants were used for CTX-I ELISA.

CTX-I ELISA

Degradation products of C-terminal telopeptides of type I collagen (CTX-I) were quantified in culture supernatant by CrossLaps® for Culture (CTX-I) ELISA (Immunodiagnostic Systems), according to the manufacturers' instructions.

In vitro TRAP staining

Osteoclasts were obtained as described earlier. TRAP staining was performed according to the manufacturers instruction (Leukocyte Acid Phosphatase Kit; Sigma-Aldrich). Staining solutions were freshly prepared before use. Bright-field microscopy was done using an Axio Scan.Z1 (Zeiss, Germany). TRAP+ multinucleated cells with three or more nuclei were defined as osteoclasts.

TRAP histology

Formalin-fixed, EDTA-decalcified, paraffin-embedded mouse tissue specimens were sectioned and stained with hematoxylin and eosin and TRAP (Sigma-Aldrich), and TRAP-positive cells were quantified.

Bone microCT analysis

Microcomputed tomography (mCT) of excised femurs was carried out by a SkyScan 1172 CT scanner (Bruker, Aartselaar, Belgium), following the general guidelines used for assessment of bone microarchitecture in rodents using mCT (Bouxsein *et al*, 2010). Briefly, scanning was conducted at 50 kV, 100 mA using a 0.5-mm aluminum filter, at a resolution of 6 mm/pixel. Reconstruction of sections was achieved using the NRECON software (Bruker) with beam hardening correction set to 40%. The analysis was performed on a volume of interest within 310 slides (1.855 mm) of the trabecular region of the femur. Cortical analysis was performed on a volume of interest within 111 slides (0.608 mm) of the cortical region of the femur. Morphometric quantification of bone indices such as trabecular (or cortical) bone volume fraction (BV/TV%), bone surface density (BS/TV%), trabecular number (Tb. N; 1/mm) and trabecular separation (Tb. Sp; mm) were performed using the CT analyzer program (Bruker). The three-dimensional imaging was performed using CTVox software (Bruker). Alternatively, samples were scanned on HECTOR (Masschaele *et al*, 2013) using a directional X-ray source set at 130 kV and 10 Watt beam power with a 1 mm Aluminum filtration, with a Perkin-Elmer XRD1620 detector (PerkinElmer, Waltham, USA) measuring 40 × 40 cm and a pixel pitch of 200 μm. A total of 2,000 projections of 1 s exposure time each was recorded. Resulting scan images had a voxel size of 4 μm. Projection images were reconstructed using Octopus Software for quantification of X-ray microtomography (Vlassenbroeck *et al*, 2007), and 3D visualizations were made using the commercial rendering software VGStudioMAX (Volume Graphics, Heidelberg, Germany). Analysis of bone morphology was performed using a custom script in ImageJ. A tibial region of interest (ROI) with a length of 1,200 μm was manually defined, starting 200 μm below the growth plate. The bone structures within this ROI were then automatically classified using an algorithm similar to that of Buie *et al* (2007). For quantification purposes, we measured both the average thickness of these structures using the Thickness plugin from BoneJ and their entire volume (determined by the number of voxels). The trabecular spacing measure is the average thickness of the nonbone volume between the trabeculae.

Mechanical testing

Mouse femurs were collected and cleaned from soft tissue. The strength of the femoral diaphysis was determined by a three-point bending test on a Lloyd Instruments universal testing machine (LRXplus, Lloyd Instruments, Fareham, UK). For this, a loading point is applied on the mid-diaphysis of the femur and is moved downward with increasing force and displacement. The maximum force (Newton) reflects the load applied right before the femur fractures.

Quantitative real-time PCR

Total RNA was isolated from cells or from total ankle tissue (crushed in liquid nitrogen) using TRIzol reagent (Invitrogen) and Aurum Total RNA Isolation Mini Kit (Biorad), according to the manufacturer's instructions. Synthesis of cDNA was performed using SensiFAST™ cDNA Synthesis Kiy according to the manufacturer's

instructions. cDNA was amplified for quantitative PCR in a total volume of 5 μl with SensiFAST SYBR® No-ROX Kit (Bioline) and specific primers on a LightCycler 480 (Roche). The reactions were performed in triplicates. The following mouse-specific primers were used: *A20* fwd AAACCAATGGTGATGGAAACTG; *A20* rev GTTGTCCCATTCGTCATTCC; *OC-Stamp* fwd TGGGCCTCCATAT GACCTCGAGTAG; *OC-Stamp* rev TCAAAGGCTTGTAAATTGGAG GAGT; *TRAP* fwd TGGTCCAGGAGCTTAACTGC; *TRAP* rev GTCAG GAGTGGGAGCCATATG; *Ctsk* fwd AGGCATTGACTCTGAAGATGC T; *Ctsk* rev TCCCCACAGGAATCTCTCTG; *RANK* fwd ATGAGTA CACGGACCGGCC; *RANK* rev GCTGGATTAGGAGCAGTGAACC; *NFATc1* fwd AGGCTGGTCTTCCGAGTTCA; *NFATc1* rev ACCGCTGG GAACACTCGAT; *HPRT* fwd AGTGTTGGATACAGGCCAGAC; *HPRT* rev CGTGATTCAAATCCCTGAAGT; *cFms* fwd TGGCATCTGGCT TAAGGTGAA; *cFms* rev GAATCCGCACCAGCTTGCTA; *IL-6* fwd GAGGATACCACTCCCAACAGACC; *IL-6* rev AAGTGCATCATCGT TGTTCATACA; *IL-1β* fwd TGGGCCTCAAAGGAAAGA *IL-1β* rev GGTGCTGATGTACCAGTT *TNF* fwd ACCCTGGTATGAGCCCA TATAC; and *TNF* rev ACACCCATTCCCTTCACAGAG.

Cytokine detection

Cytokine levels in culture medium were determined by magnetic bead-based multiplex assay using Luminex technology (Bio-Rad), according to the manufacturers' instructions.

Western blotting

Cells were lysed directly in 2 × Laemlli and boiled for 5 min. Lysates were separated by SDS polyacrylamide gel electrophoresis, transferred to nitrocellulose membranes with a semi-dry blot system (Invitrogen), and immunoblotted with anti-IκBα (Santa Cruz Biotechnology, Inc., sc-371), anti-phospho-IκBα (Cell Signaling, CST9246), anti-A20 (Santa Cruz Biotechnology, Inc., sc-166692), anti-p38 (Cell Signaling, CST9212), anti-phospho-p38 (Cell Signaling, CST9215), anti-SAPK/JNK (Cell Signaling, CST9252), anti-phospho-SAPK/JNK (Cell Signaling, CST4668), anti-NF-kB2 p100/p52 (Cell Signaling, CST4882), anti-TRAF6 (MBL, MBL597), anti-HOIP (Abcam, ab46322), anti-Sharpin (Proteintech, 14626-1-AP), anti-RANK (Santa Cruz Biotechnology, Inc., sc-374360), anti-p65 (Santa Cruz Biotechnology, Inc., sc-8008), anti-phospho-p65 (Cell Signaling, CST3033), and anti-β-actin (Santa Cruz Biotechnology, Inc., sc-47778) antibodies. Individual membranes may have been reprobed with different antibodies.

NF–κB-dependent reporter assays

Human embryonic kidney (HEK293T) cells were seeded at 2×10^5 cells/well in 6-well plates. Cells were transiently transfected the next day by DNA calcium phosphate coprecipitation. Each transfection contained 100 ng of pNFconluc, 100 ng pactβgal, 100 ng of a RANK expression vector, and 100 ng of a specific pCAGGS-A20 expression plasmid (expressing wild-type human A20 or the indicated DUB (C103A), ZnF4 (C624A–C627A), ZnF7 (C775A–C779A), or ZnF4ZnF7 (C624A–C627A/C775A–C779A) mutants). The total amount of DNA per well was kept constant at 1 μg by adding an empty pCAGGS vector. After 24 h, cells were lysed in luciferase lysis buffer (25 mM Tris phosphate pH 7.8; 2 mM DTT; 2 mM CDTA(1,2

diaminocyclohexane-N.N.N.N-tetraacetic acid); 10% glycerol; 1% Triton X-100). Substrate buffer was added (658 mM luciferin, 378 mM coenzyme A and 742 mM ATP), and Luciferase activity (Luc) was assayed in a GloMax 96 Microplate Luminometer (Promega). β-Galactosidase (βgal) activity in cell extracts was assayed with the chlorophenol-red β-D-galactopyranoside substrate (Roche Applied Science, Basel, Switzerland), and the optical density was read at 595 nm in a Benchmark microplate Reader (Bio-Rad Laboratories, Nazareth, Belgium). Luc values were normalized for βgal values to correct for differences in transfection efficiency (plotted as Luc/βgal). The data represent the average ± SD of technical triplicates.

A20-GST pulldown assays

BMDMs were pretreated for 1 h with 50 μM HOIPIN-8 (Axon Medchem) or left untreated and stimulated with GST–RANKL (1 μg/ml; VIB Protein Service Facility), as indicated. Cells were lysed in NP40 buffer (150 mM NaCl, 1% NP40, 10% glycerol and 10 mM Tris–HCl pH 8) and GST pulldown was performed using glutathione sepharose 4B (Sigma).

Statistics

GraphPad Prism V8 software was used for statistical analysis. Results are expressed as the mean ± SEM or mean ± SD, as indicated in the figure legend. Statistical significance between experimental groups was assessed using a nonparametric Mann–Whitney *U*-statistical test. Statistical significance between multiple groups was assessed using either one- or two–way ANOVA with Tukey correction for multiple comparison. No animals or samples were excluded from any analysis.

Data availability

No primary datasets have been generated and deposited.

Expanded View for this article is available online.

Author contributions

Arne Martens: Conceptualization; data curation; formal analysis; investigation; methodology; writing – original draft. **Pieter Hertens:** Data

curation; formal analysis; investigation; methodology. **Dario Priem:** Data curation; formal analysis; investigation; methodology. **Vagelis Rinotas:** Data curation; formal analysis; investigation; methodology. **Theodore Meletakos:** Data curation; formal analysis; investigation; methodology. **Meropi Gennadi:** Data curation; formal analysis; investigation; methodology. **Lisette van Hove:** Data curation; formal analysis; investigation. **Els Louagie:** Data curation; formal analysis; investigation. **Julie Coudenys:** Data curation; formal analysis; investigation. **Amélie De Muynck:** Data curation; formal analysis; investigation. **Djoere Gaublomme:** Data curation; software. **Mozes Sze:** Data curation; formal analysis; investigation. **Jolanda Van Hengel:** Resources; methodology. **Leen Catrysse:** Data curation; formal analysis; investigation. **Esther Hoste:** Data curation; formal analysis; investigation. **Jeffrey D Zajac:** Resources. **Rachel Davey:** Resources. **Luc Van Hoorebeke:** Resources; supervision; methodology. **Tino Hochepied:** Resources; investigation; methodology. **Mathieu JM Bertrand:** Formal analysis; supervision; investigation; methodology. **Maria Armaka:** Formal analysis; supervision; investigation; methodology. **Dirk Elewaut:** Formal analysis; supervision; investigation; methodology. **Geert van Loo:** Conceptualization; data curation; formal analysis; supervision; funding acquisition; investigation; methodology; writing – original draft; project administration; writing – review and editing.

Disclosure and competing interests statement

References

Asagiri M, Takayanagi H (2007) The molecular understanding of osteoclast differentiation. *Bone* 40: 251–264

Boone DL, Turer EE, Lee EG, Ahmad RC, Wheeler MT, Tsui C, Hurley P, Chien M, Chai S, Hitotsumatsu O *et al* (2004) The ubiquitin-modifying enzyme A20 is required for termination of toll-like receptor responses. *Nat Immunol* 5: 1052–1060

Bouxsein ML, Boyd SK, Christiansen BA, Guldberg RE, Jepsen KJ, Muller R (2010) Guidelines for assessment of bone microstructure in rodents using micro-computed tomography. *J Bone Miner Res* 25: 1468–1486

Boyle WJ, Simonet WS, Lacey DL (2003) Osteoclast differentiation and activation. *Nature* 423: 337–342

Buie HR, Campbell GM, Klinck RJ, MacNeil JA, Boyd SK (2007) Automatic segmentation of cortical and trabecular compartments based on a dual threshold technique for in vivo micro-CT bone analysis. *Bone* 41: 505–515

Chang J, Wang Z, Tang E, Fan Z, McCauley L, Franceschi R, Guan K, Krebsbach PH, Wang CY (2009) Inhibition of osteoblastic bone formation by nuclear factor-kappaB. *Nat Med* 15: 682–689

Chiu WS, McManus JF, Notini AJ, Cassady AI, Zajac JD, Davey RA (2004) Transgenic mice that express Cre recombinase in osteoclasts. *Genesis* 39: 178–185

Clausen BE, Burkhardt C, Reith W, Renkawitz R, Forster I (1999) Conditional gene targeting in macrophages and granulocytes using LysMcre mice. *Transgenic Res* 8: 265–277

Dai J, Lin D, Zhang J, Habib P, Smith P, Murtha J, Fu Z, Yao Z, Qi Y, Keller ET (2000) Chronic alcohol ingestion induces osteoclastogenesis and bone loss through IL-6 in mice. *J Clin Invest* 106: 887–895

De A, Dainichi T, Rathinam CV, Ghosh S (2014) The deubiquitinase activity of A20 is dispensable for NF-kappaB signaling. *EMBO Rep* 15: 775–783

Draber P, Kupka S, Reichert M, Draberova H, Lafont E, de Miguel D, Spilgies L, Surinova S, Taraborrelli L, Hartwig T *et al* (2015) LUBAC-recruited CYLD and A20 regulate gene activation and cell death by

exerting opposing effects on linear ubiquitin in signaling complexes. *Cell Rep* 13: 2258–2272

Itzstein C, Coxon FP, Rogers MJ (2011) The regulation of osteoclast function and bone resorption by small GTPases. *Small GTPases* 2: 117–130

Jin W, Chang M, Paul EM, Babu G, Lee AJ, Reiley W, Wright A, Zhang M, You J, Sun SC (2008) Deubiquitinating enzyme CYLD negatively regulates RANK signaling and osteoclastogenesis in mice. *J Clin Invest* 118: 1858–1866

Ju JH, Cho ML, Moon YM, Oh HJ, Park JS, Jhun JY, Min SY, Cho YG, Park KS, Yoon CH *et al* (2008) IL-23 induces receptor activator of NF-kappaB ligand expression on CD4+ T cells and promotes osteoclastogenesis in an autoimmune arthritis model. *J Immunol* 181: 1507–1518

Kasher M, Freidin MB, Williams FM, Cherny SS, Malkin I, Livshits G (2021) Shared genetic architecture between rheumatoid arthritis and varying osteoporotic phenotypes. *J Bone Miner Res* 37: 440–453

Krikos A, Laherty CD, Dixit VM (1992) Transcriptional activation of the tumor necrosis factor alpha-inducible zinc finger protein, A20, is mediated by kappa B elements. *J Biol Chem* 267: 17971–17976

Lam J, Takeshita S, Barker JE, Kanagawa O, Ross FP, Teitelbaum SL (2000) TNF-alpha induces osteoclastogenesis by direct stimulation of macrophages exposed to permissive levels of RANK ligand. *J Clin Invest* 106: 1481–1488

Lee EG, Boone DL, Chai S, Libby SL, Chien M, Lodolce JP, Ma A (2000) Failure to regulate TNF-induced NF-kappaB and cell death responses in A20-deficient mice. *Science* 289: 2350–2354

Levescot A, Chang MH, Schnell J, Nelson-Maney N, Yan J, Martinez-Bonet M, Grieshaber-Bouyer R, Lee PY, Wei K, Blaustein RB *et al* (2021) IL-1beta-driven osteoclastogenic Tregs accelerate bone erosion in arthritis. *J Clin Invest* 131: e141008

Lippens S, Lefebvre S, Gilbert B, Sze M, Devos M, Verhelst K, Vereecke L, Mc Guire C, Guerin C, Vandenabeele P *et al* (2011) Keratinocyte-specific ablation of the NF-kappaB regulatory protein A20 (TNFAIP3) reveals a role in the control of epidermal homeostasis. *Cell Death Differ* 18: 1845–1853

Lombardi L, Ciana P, Cappellini C, Trecca D, Guerrini L, Migliazza A, Maiolo AT, Neri A (1995) Structural and functional characterization of the promoter regions of the NFKB2 gene. *Nucleic Acids Res* 23: 2328–2336

Martens A, Priem D, Hoste E, Vetters J, Rennen S, Catrysse L, Voet S, Deelen L, Sze M, Vikkula H *et al* (2020) Two distinct ubiquitin-binding motifs in A20 mediate its anti-inflammatory and cell-protective activities. *Nat Immunol* 21: 381–387

Martens A, van Loo G (2020) A20 at the crossroads of cell death, inflammation, and autoimmunity. *Cold Spring Harb Perspect Biol* 12: a036418

Masschaele B, Dierick M, Loo DV, Boone MN, Brabant L, Pauwels E, Cnudde V, Hoorebeke LV (2013) HECTOR: A 240kV micro-CT setup optimized for research. *JPCS* 463: 012012

Matmati M, Jacques P, Maelfait J, Verheugen E, Kool M, Sze M, Geboes L, Louagie E, Mc Guire C, Vereecke L *et al* (2011) A20 (TNFAIP3) deficiency in myeloid cells triggers erosive polyarthritis resembling rheumatoid arthritis. *Nat Genet* 43: 908–912

Novack DV (2011) Role of NF-kappaB in the skeleton. *Cell Res* 21: 169–182

Plenge RM, Cotsapas C, Davies L, Price AL, de Bakker PI, Maller J, Pe'er I, Burtt NP, Blumenstiel B, DeFelice M *et al* (2007) Two independent alleles at 6q23 associated with risk of rheumatoid arthritis. *Nat Genet* 39: 1477–1482

Polykratis A, Martens A, Eren RO, Shirasaki Y, Yamagishi M, Yamaguchi Y, Uemura S, Miura M, Holzmann B, Kollias G *et al* (2019) A20 prevents inflammasome-dependent arthritis by inhibiting macrophage necroptosis through its ZnF7 ubiquitin-binding domain. *Nat Cell Biol* 21: 731–742

Priem D, Devos M, Druwe S, Martens A, Slowicka K, Ting AT, Pasparakis M, Declercq W, Vandenabeele P, van Loo G *et al* (2019) A20 protects cells from TNF-induced apoptosis through linear ubiquitin-dependent and -independent mechanisms. *Cell Death Dis* 10: 692

Quinn JM, Elliott J, Gillespie MT, Martin TJ (1998) A combination of osteoclast differentiation factor and macrophage-colony stimulating factor is sufficient for both human and mouse osteoclast formation in vitro. *Endocrinology* 139: 4424–4427

Sun SC (2017) The non-canonical NF-kappaB pathway in immunity and inflammation. *Nat Rev Immunol* 17: 545–558

Takayanagi H, Kim S, Koga T, Nishina H, Isshiki M, Yoshida H, Saiura A, Isobe M, Yokochi T, Inoue J *et al* (2002) Induction and activation of the transcription factor NFATc1 (NFAT2) integrate RANKL signaling in terminal differentiation of osteoclasts. *Dev Cell* 3: 889–901

Thomson W, Barton A, Ke X, Eyre S, Hinks A, Bowes J, Donn R, Symmons D, Hider S, Bruce IN *et al* (2007) Rheumatoid arthritis association at 6q23. *Nat Genet* 39: 1431–1433

Tokunaga F, Nishimasu H, Ishitani R, Goto E, Noguchi T, Mio K, Kamei K, Ma A, Iwai K, Nureki O (2012) Specific recognition of linear polyubiquitin by A20 zinc finger 7 is involved in NF-kappaB regulation. *EMBO J* 31: 3856–3870

Tsukasaki M, Takayanagi H (2019) Osteoimmunology: evolving concepts in bone-immune interactions in health and disease. *Nat Rev Immunol* 19: 626–642

Vande Walle L, Van Opdenbosch N, Jacques P, Fossoul A, Verheugen E, Vogel P, Beyaert R, Elewaut D, Kanneganti TD, van Loo G *et al* (2014) Negative regulation of the NLRP3 inflammasome by A20 protects against arthritis. *Nature* 512: 69–73

Vereecke L, Sze M, Mc Guire C, Rogiers B, Chu Y, Schmidt-Supprian M, Pasparakis M, Beyaert R, van Loo G (2010) Enterocyte-specific A20 deficiency sensitizes to tumor necrosis factor-induced toxicity and experimental colitis. *J Exp Med* 207: 1513–1523

Verhelst K, Carpentier I, Kreike M, Meloni L, Verstrepen L, Kensche T, Dikic I, Beyaert R (2012) A20 inhibits LUBAC-mediated NF-kappaB activation by binding linear polyubiquitin chains via its zinc finger 7. *EMBO J* 31: 3845–3855

Vlassenbroeck J, Dierick M, Masschaele B, Cnudde V, Hoorebeke LV, Jacobs P (2007) Software tools for quantification of X-ray microtomography at the UGCT. *Nucl Instrum Methods Phys Res* 580: 442–445

Wada T, Nakashima T, Hiroshi N, Penninger JM (2006) RANKL-RANK signaling in osteoclastogenesis and bone disease. *Trends Mol Med* 12: 17–25

Zaidi M (2007) Skeletal remodeling in health and disease. *Nat Med* 13: 791–801

Zhang SQ, Kovalenko A, Cantarella G, Wallach D (2000) Recruitment of the IKK signalosome to the p55 TNF receptor: RIP and A20 bind to NEMO (IKKgamma) upon receptor stimulation. *Immunity* 12: 301–311